Electronic Supplementary Information

Contactless conductivity biosensor in microchip containing folic acid as bioreceptor

Renato S. Lima,[a,b] Maria H. O. Piazzetta,[c] Ângelo L. Gobbi,[c] Ubirajara P. Rodrigues-Filho,[a] Pedro A. P. Nascente,[d] Wendell K. T. Coltro,[e] and Emanuel Carrilho[*a,b]

[a] *Instituto de Química de São Carlos, Universidade de São Paulo, São Carlos, SP, Brazil;*
[b] *Instituto Nacional de Ciência e Tecnologia de Bioanalítica, Campinas, SP, Brazil;*
[c] *Laboratório Nacional de Nanotecnologia, Centro Nacional de Pesquisa em Energia e Materiais, Campinas, SP, Brazil;*
[d] *Departamento de Engenharia de Materiais, Universidade Federal de São Carlos, SP, Brazil.*
[e] *Instituto de Química, Universidade Federal de Goiás, GO, Brazil.*
*emanuel@iqsc.usp.br

Material and methods

Ethanol, acetone, acetonitrile, sulfuric acid (H_2SO_4), and hydrogen peroxide (H_2O_2) were supplied from Synth (Diadema, Brazil). Lithium perchlorate ($LiClO_4$), 4-(triethoxysilyl) butyronotrile (ButCN), 3-(aminopropyl)triethoxysilane (APTS), folic acid (FA), TRIS buffered saline (TBS), MES, monoclonal antibody against FA (α-FA), N,N'-dicyclohexylcarbodiimide (DCC), dimetilsulfoxide (DMSO), and pyridine were purchased from Sigma-Aldrich Chemical Co. (MO, USA). All solutions were prepared utilizing deionized water (Milli-Q, Bedford, USA) with resistivity no less than 18 MΩ cm.

The analytical instrumentation required by μBIA-C^4D consisted of the following components: *i)* alternating signal generator (Minipa MFG 4202, São Paulo, Brazil), *ii)* conductivity detector, whose electronic circuit was home-designed and built according to a previously reported scheme,[1] and *iii)* two syringe-pumps for microfluidic handling (New Era Pump Systems Inc. NE-300, Farmingdale, NY).

Using a program written in LabVIEW carried out the data acquisition. Teflon reactors (8.0 cm internal diameter and 2.0 cm depth) were used for the surface functionalization reactions. These reactors, as all employed glassware, were previously washed in H_2SO_4/H_2O_2 (3:1, v/v) solution for 30 min and abundant deionized water. Scanning electron microscopy (SEM) images of the modified surfaces were carried out in a Carl Zeiss LEO 440 microscope (NY, USA). This instrument operated with tungsten thermionic filament, 20 kV potential, sample chamber under high vacuum (pressure of 1 Pa), and secondary electron detector as analytical mode. X-ray photoelectron spectroscopy (XPS) measurements were performed from a Kratos Analytical XSAM HS spectrometer (Chestnut Ridge, NY), operating with non-monochromatic Mg Kα radiation (1,253.6 eV in binding energy) and flood-gun (charge neutralizer device) in order to avoid the charging of the samples.[2] The pressure in the sample chamber was in the range of 10^{-7} Pa, whereas the Shirley method was used for background subtraction. Atomic force microscopy (AFM) images were acquired in tapping mode with constant force in a Veeco MultiMode™ SPM equipment (Plainview, NJ), containing 512 x 512 pixels at maximum resolution. Finally, the thicknesses of the films were measured using a Veeco Dektak 3ST ellipsometer (New York, NY).

Optimization of the dielectric thickness

Alterations in the nature and thickness of the dielectric were carried out seeking to improve the sensitivity of the system. In these studies, flowing aqueous solutions of LiClO4 into the microchannels performed C4D flow analyses. Microdevices without the biosensor phase were used. Thus, only one of the receiver electrodes was employed (e_{wr} in Fig. 1b) during the experiments. The signals were recorded by flow analyses switching two external syringe pumps so that either water or saline solution was pumped into the microfluidic channels. First, water was circulated for approximately 5 min seeking the signal stabilization. Once a stable baseline was achieved, the samples were introduced

generating a potential change on the receiver electrode. Next, water was added resulting in a decrease of the signal nearly to its initial value. The analytical responses recorded in this study were associated to the signal difference after maximum of the signal from the sample and its baseline (water) values.

The tested dielectrics were: *i)* SiO_2 (C^4D_{SiO2}), deposited by plasma-enhanced chemical vapor deposition (PECVD) with 50-nm-thickness, and *ii)* PDMS (C^4D_{PDMS}), coated by spinning at 1000 rpm for 10 s resulting in a layer 50-µm thick. In both cases, the electrodes were made with a width and gap of 1.0 mm (Fig. 1b). The microchips were applied to $LiClO_4$ standards (25-50 µmol L^{-1} for C^4D_{SIO2} and 2-8 mmol L^{-1} for C^4D_{PDMS}); deionized water was employed as a blank. The following conditions were adopted in both cases: 400 kHz frequency, 2.5 V_{P-P} peak-to-peak voltage (V_{p-p}), 100 µLmin^{-1} flow rate, and 15 s salt-sampling time. The analytical signals and calibration curves obtained are illustrated in Fig. S1. The analysis of residues and F-test for linearity validated the linear fit for all analytical curves. The limit-of-detections (LODs), calculated using 3σ/slope ratio (σ is the standard deviation of the mean voltage for 7 measurements of the blank), were: 12.7 (C^4D_{SIO2}) and 894.6 µmol L^{-1} (C^4D_{PDMS}).

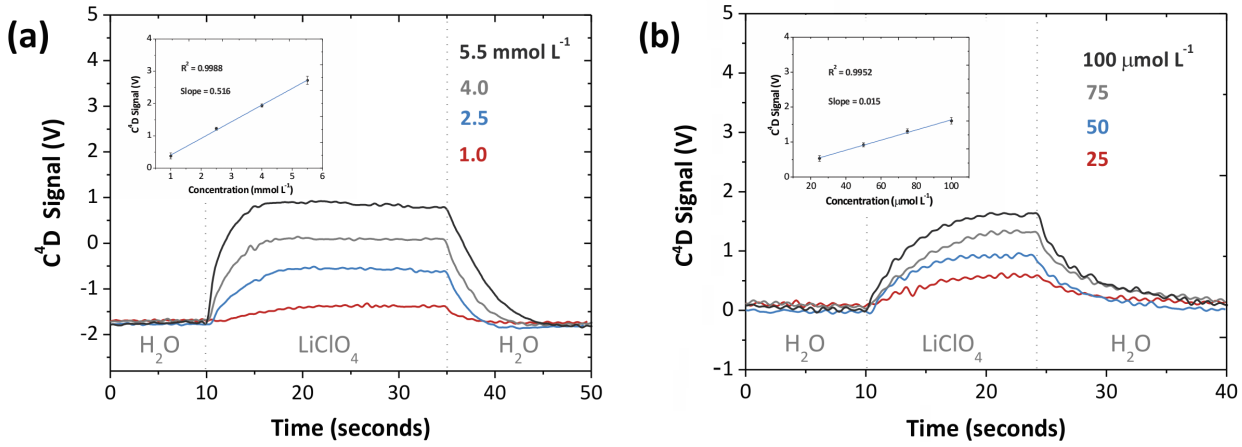

Fig. S1 Analytical signals and calibration curves (insets) obtained for C^4D_{PDMS} (a) and C^4D_{SiO2} (b) microchips.

C^4D_{SiO2} exhibited a LOD (12.7 µmol L^{-1} for $LiClO_4$) considerably smaller than that recorded for C^4D_{PDMS} (894.6 µmol L^{-1} for $LiClO_4$). SiO_2 and PDMS present similar dielectric constants, around of 4

for SiO_2 [3] and 3 for PDMS.[4] Thereby, since that the other intervenient factors in the C^4D response (nature and concentration of the solutions, dimensions of the detection cell, and gap among the electrodes) were the same for both systems, presumably the difference in the LODs values is due to the thickness values presented: 50 nm for SiO_2 and 50 µm for PDMS. The lowest thicknesses of SiO_2 provided a reduction in resistivity imposed on the capacitive coupling electrode/solution, increasing the capacitance recorded by the receiver electrode as discussed with more details in the following section.[5] Here, the SiO_2 film was employed in the further experiments.

The use of a nanometric film for electrical insulation of the electrodes in µBIA-C^4D represents a substantial advantage regarding the majority of other published C^4D microchips. Commonly, the thicknesses of the insulating layer for C^4D microdevices range from tens to hundreds of micrometers.[6]

Effect of the area on the response in C^4D

The area affects the C^4D signal by increasing the conductance and capacitance parameters as discussed below.

C^4D signal

The output voltage of the C^4D amplifier ($\boldsymbol{V_{out}}$) directly varies with the conductance of the electrolyte and the equivalent capacitance of the of the detector ($\boldsymbol{C}$) according to equation (1).[7]

$$\boldsymbol{V_{out}} = \frac{\boldsymbol{V_{in}}}{\boldsymbol{1} + \boldsymbol{j2\pi fRC_o}} \boldsymbol{R_f} \qquad (1)$$
$$\boldsymbol{j2\pi(C + C_o)}\left(1 + \frac{j2\pi fRCC_o}{C + C_o}\right)$$

being V_{in} the input voltage, j an imaginary unit, f the frequency of the RF signal, R_f the feedback resistance on the amplifier, R the cell resistance (inverse of conductance), and C_o the stray capacitance as above mentioned. Below we discuss the variations of the C^4D response with the conductance and capacitance parameters.

Variation of the C^4D signal with the conductance

In conductommetry, with and without contact, the mass transport phenomenon intervenient in the analytical response is the migration. The contribution of the difusional processes is minimized by applying an alternating signal, usually with sine waves,[8] to the excitation electrode. Under these conditions, the particles oscillate around a given mean position, preventing the formation of a resulting concentration gradient ($\partial c/\partial x$). Therefore, the diffusion flow (J_D) is eliminated according the Fick's first law:[9]

$$J_D = -D\frac{\partial c}{\partial x} \tag{2}$$

in which D is the diffusion coefficient of the species. In this context, the response in conductommetry is closely related to the migration flow of the ions in solution (J_M). This parameter is directly dependent on the equilibrium concentration (c_j), the effective ion mobility (μ_j) of the species, and the electric potential generated between the electrodes ($\partial\phi/\partial x$) as shown in equation (3):[10]

$$J_M = -(\sum_j c_j \mu_j)\frac{\partial \phi}{\partial x} \tag{3}$$

The migrational current (i_M) generated at a conductivity cell is proportional to the flow rate, which measures the number of particles that cross a given area per unit time, to the module of the charge of the electrolyte ($|z_j|$), and to the detection area A. Mathematically, we have:

$$\boldsymbol{i_M} = -J_M FA\sum_j |z_j| \tag{4}$$

being ***F*** the Faraday constant. Substituting (3) in (4):

$$\boldsymbol{i_M} = FA(\sum_j c_j |z_j| \mu_j)\frac{\partial \phi}{\partial x} \tag{5}$$

Neglecting the edge effects of the electric field, this field (***ΔE***) will be linear throughout the detection cell. Under these conditions:[11]

$$\frac{\partial \phi}{\partial x} = \frac{\Delta E}{l} \tag{6}$$

where ***l*** is the distance between the electrodes. Substituting (6) in (5):

$$\boldsymbol{i_M} = F\left(\frac{A}{l}\right)(\sum_j c_j |z_j| \mu_j)\Delta E \tag{7}$$

The ***A/l*** ratio is known as cell constant. From Ohm's law:[10]

$$\boldsymbol{i_M} = \frac{\Delta E}{R} \tag{8}$$

being ***R*** the resistance imposed to the charge transport among the electrodes. Applying (8) in (7):

$$\frac{1}{R} = F\left(\frac{A}{l}\right)(\sum_j c_j |z_j| \mu_j) \tag{9}$$

The inverse of resistance is called conductance, $\boldsymbol{L}$ (Ω^{-1}), so that this parameter increases with the cell constant and the linear combination of the contributions from all ions present in the sample. Such contributions take into account the equilibrium concentration ($\boldsymbol{c_i}$) and the nature of these ions ($\boldsymbol{z_i}$ e $\boldsymbol{u_i}$) as shown in equation (10):[10]

$$L = F\left(\frac{A}{l}\right)\left(\sum_j c_j \mid z_j \mid \mu_j\right) \tag{10}$$

with,

$$L = \kappa\left(\frac{A}{l}\right) \tag{11}$$

where $\boldsymbol{\kappa}$, called conductivity (Ω^{-1} cm^{-1}), is the proportionality constant between $\boldsymbol{L}$ and the cell constant. This parameter is an intensive property and given by:

$$\kappa = F\left(\sum_j c_j \mid z_j \mid \mu_j\right) \tag{12}$$

As it can be observed in equation (1), keeping constant the frequency of operation, the detector electronics, and the geometry of the conductivity cell (affects $\boldsymbol{C}$ and $\boldsymbol{C_o}$), the variations in $\boldsymbol{V_{out}}$ will occur as function of the values of conductance. Studies show that there is a linear relation among the C^4D signals (in volts) and $\boldsymbol{\kappa}$ in the range of 0.2 to 1.5 mS cm^{-1}. The solutions used in conductommetric determinations, with and without contact, usually present conductivities in this range.[7]

The C^4D sensitivity increases with the sensing area as shown in equation (10), from which it can be observed that $\boldsymbol{L}$ directly depends on $\boldsymbol{A}$. This phenomenon can be explained according to the

raising in concentration of charge carriers between the electrodes, increasing consequently the resulting conductance values. The effect of the electrodes area on the analytical response in C^4D was demonstrated by Lee and *et al.* in 2006.[12] Electrophoretic signals to Rhodamine B samples were recorded by microdevices incorporating planar and semicircular electrodes. The latter resulted in capacitance intensities more than four times compared to those obtained with planar electrodes. Nevertheless, it is important to highlight that the simple increase of this area by the electrode width does not necessarily improve the signal-to-noise (S/N) ratio in C^4D. Data show that widths greater than 2 mm, although have increased in capacitance, result in signal reduction due to the parallel increase in noise that occurs as function of the stray capacitance. This parameter arises from direct capacitive coupling between the electrodes.[7]

Variation of the C^4D signal with the capacitance

Consider the Gauss's law to mathematical description of $\boldsymbol{C}$. Briefly, the electric field generated by the electrode/dielectric/solution systems ($\boldsymbol{E_C}$) is obtained from a Gaussian surface enclosing all the charge $\boldsymbol{q}$ on any one of the plates of the capacitor (electrode and solution in C^4D), as illustrates the equation (13).[10,11]

$$\varepsilon\varepsilon_o \oint \vec{E}_C \, d\,\vec{A} = q \qquad (13)$$

being $\boldsymbol{A}$ the area of each one of these plates (sensing area in C^4D), $\boldsymbol{\varepsilon}$ the dielectric constant of the material that insulates the electrodes, and $\boldsymbol{\varepsilon_o}$ the permittivity constant of the free space (8.85 pF m^{-1}). When the plates are very close to each other, we can neglect the edge effect of the electric field. Therefore, $\boldsymbol{E_C}$ will be linear throughout the Gaussian surface so that equation (13) reduces to:

$$E_C = \frac{q}{\varepsilon\varepsilon_o A} \tag{14}$$

For a linear electric field:

$$V = E_C \int_0^d dS = E_C d \tag{15}$$

In this equation, ***d*** is the distance between the plates and ***dS*** is the displacement vector. On the other hand, the capacitance (***C***) represents the ability of a system for accumulating charges (***q***) under a given applied potential (***V***). Mathematically, we have:

$$C = \frac{q}{V} \tag{16}$$

Substituting (14) and (15) in (16), the following equation for capacitance is achieved according to Gauss' law:

$$C = \frac{\varepsilon\varepsilon_o A}{d} \tag{17}$$

Based on equation (17), we can to verify that ***C*** changes directly and indirectly with the electrode area and the dielectric thicknesses, respectively. For a better understanding about the phenomenon responsible for these variations, let us consider a capacitor connected to a battery as shown in Scheme S1a. Since connecting the capacitor, initially uncharged, to the battery, electrons (charge carriers) flow through conducting wires according to a direction determined by the battery

electric field (E_B). Due to the charging process of the capacitor plates (electrode and solution in C^4D), an electric field ($\boldsymbol{E_C}$) contrary to E_B is formed whose magnitude is given by equation (14). When there is a dielectric between the capacitor plates, $\boldsymbol{C}$ increases as a numerical factor called dielectric constant (equation 17).[11]

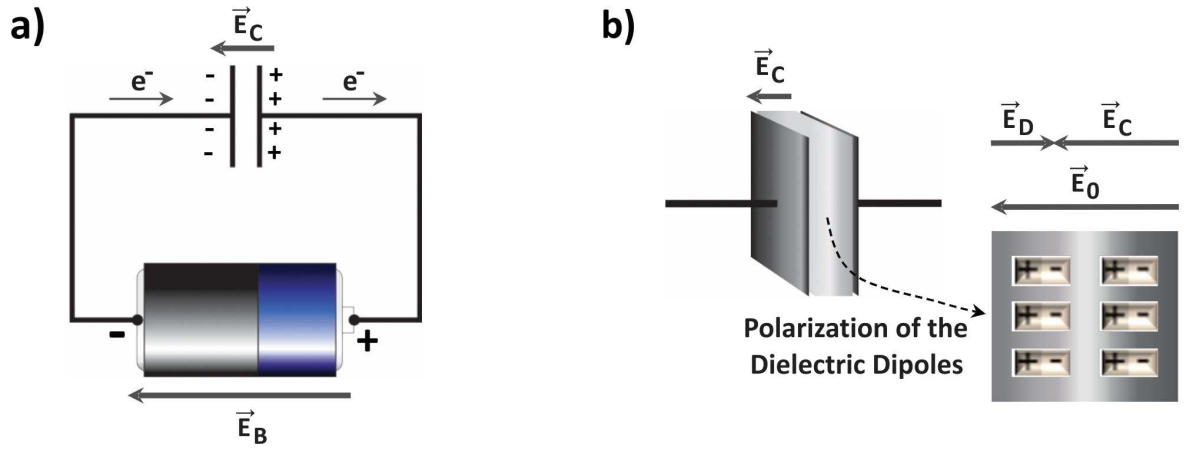

Scheme S1 Schematic diagrams with (a) the elements of an electrical circuit incorporating capacitor and battery and (b) the polarization phenomenon of the charge centers (+/-) of the dielectric in capacitors. E_B, E_D, E_0, and E_C, electric fields of the battery, dielectric, initial value of the capacitor, and the resulting electric field of the capacitor, respectively. Figure adapted from reference 5 with permission.

In atomic and molecular terms, what causes such increase? The dielectric constant of the insulating material expresses the polarization ability of its charge centers under an electric field. Regardless of whether they have permanent electric dipole moments (polar and polarizable dipole) or not, the molecules that constitute the dielectric acquire these moments by induction of its positive and negative charge centers when exposed to an external electric field. The phenomenon of dipole polarization, shown in Scheme S1b, induces an electric field (E_D) less intense and contrary to the capacitor initial field (E_0, hypothetical value for the capacitor without dielectric). Thus, E_0 is reduced to a resulting field ($\boldsymbol{E_C}$) as a magnitude given by the $\boldsymbol{P}$ parameter, denominated dielectric polarization and calculated as follows:[13]

$$P = \frac{\varepsilon - 1}{\varepsilon} \tag{18}$$

Since $\boldsymbol{E_C}$ is opposed to the battery field, the charging process of the capacitor has increased its efficiency with a consequent raise in equilibrium capacitance.[11]

Similarly to what occurs with electrical capacitors, in C^4D the increment in the capacitance values of the electrode/dielectric/solution systems is due primarily to a reduction in $\boldsymbol{E_C}$, which arises from a more effective polarization of the dielectric molecules. The efficiency of this polarization process is expressed by $\boldsymbol{\varepsilon}$ and it is also affected by the $\boldsymbol{A}$ and $\boldsymbol{d}$ parameters. Thus, the increase in capacitance with the electrode area can be explained based on the intensification of the dielectric molecules polarization, resulting in a decrease of $\boldsymbol{E_C}$. On the other hand, the reduction in capacitance facing to the dielectric thickness occurs thanks to the increase in the number of interactions/collisions between the dielectric molecules during the polarization process.[11] This phenomenon reduces the electric field related to the insulating material E_D, increasing thus the capacitor field. According to data in the literature,[14] there is a loss of approximately 75% in analytical signal when $\boldsymbol{d}$ is increased from 125 to 425 µm.

Optimization of the silanization conditions

As highlighted in main text, the silanized surfaces were characterized by scanning electron microscopy (SEM) and X-ray photoelectron spectroscopy (XPS) measurements. SEM was used in order to checking the formation of clusters, whereas XPS was employed for qualitative and quantitative determinations of the modified surfaces. This allowed us to ascertain the adsorption rate of the silanes. Table S1 summarizes the parameters used in the assays, which were intended to optimize the silanization conditions.

Table S1 Reactional conditions studied for silanization of the SiO_2 film

Condition	*Silane*	*Concentration*	*Solvent*	*Reaction Time (min)*
SAM A.1	ButCN	1 mmol L^{-1}	Acetonitrile	60
SAM A.2	ButCN	1 mmol L^{-1}	Acetonitrile	150
SAM A.3	ButCN	1 mmol L^{-1}	Acetonitrile	300
SAM B.1	APTS	1 mmol L^{-1}	Acetone	60
SAM B.2	APTS	1 mmol L^{-1}	Acetone	120
SAM B.3	APTS	1 mmol L^{-1}	Acetone	180
SAM C.1	APTS	3% (v/v)	Ethanol	180
SAM C.2	APTS	3% (v/v)	Ethanol	300

As a didactic example, Fig. S2a shows clusters formed on a SiO_2 film modified with 3-imidazolilpropyltrimethoxysilane (3-IUTS), 1 mmol L^{-1} in toluene, for 150 min. Meanwhile, for all conditions investigated in this paper, the SEM images did not indicate clustering to 3 µm, 1 µm, and 200 nm resolution levels. The SEM images were recorded at four different and random points for each sample. Fig. S2b shows the SEM image of the silanization condition SAM C.2.

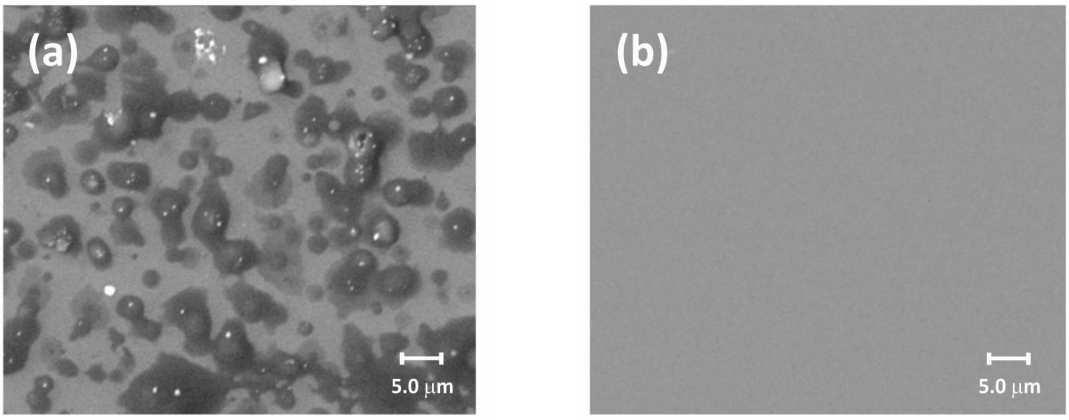

Fig. S2 Assessment of the formation of clusters on the silanized SiO_2 surface. SEM images corresponding to surfaces modified with 1 mmol L^{-1} 3-IUTS in toluene for 150 min (a) and 3% APTS in ethanol (v/v) for 24 h (b).

Fig. S3 shows the XPS spectra corresponding to the Si 2p peak achieved for the SAM C.2-modified SiO_2 surface.

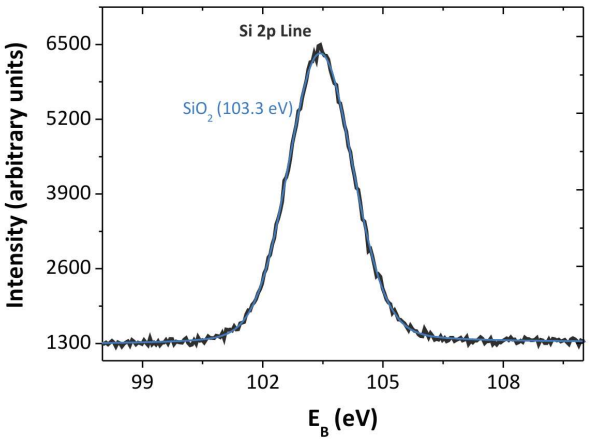

Fig. S3 XPS spectra of the Si 2p peak obtained for SAM C.2-modified (Table 1 in the communication) SiO_2 surface. The binding energy (E_B, eV) is reported in parentheses for the SiO_2 component.

Fig. S4a–c detail XPS spectra (exploratory and N 1s lines) obtained to modified SiO_2 films using the SAM C.2 and SAM A.3 conditions. Fig. S4d, in turn, illustrates the N/Si ratios whose values were similar for SAMs A and B. Presumably, this fact is due to saturation of the silanol groups of the SiO_2 surface available for silanization.[15] Concerning the samples modified with SAM C, there was a reasonable increase in the silanization efficiency with the reactional time. Based on the results, we adopted APTS under the SAM C.2 conditions as FA-immobilization intermediary in subsequent analyses.

FA-functionalization protocol

Briefly, FA in excess (approximately 515 mg) was dissolved in DMSO (50 mL) at temperatures between 40 and 45 ^{o}C. Then, pyridine (515 μL) and DCC (412 μL) were added to this mixture. DCC functions as a heterobifunctional crosslinker between the groups amine of the silane and carboxyl of the FA groups.[16] Finally, the APTS-silanized SiO_2 surface was incubated in this FA solution for different times at 40–45 ^{o}C. Three FA-functionalization times were explored, namely: 3, 5, and 7 hr.

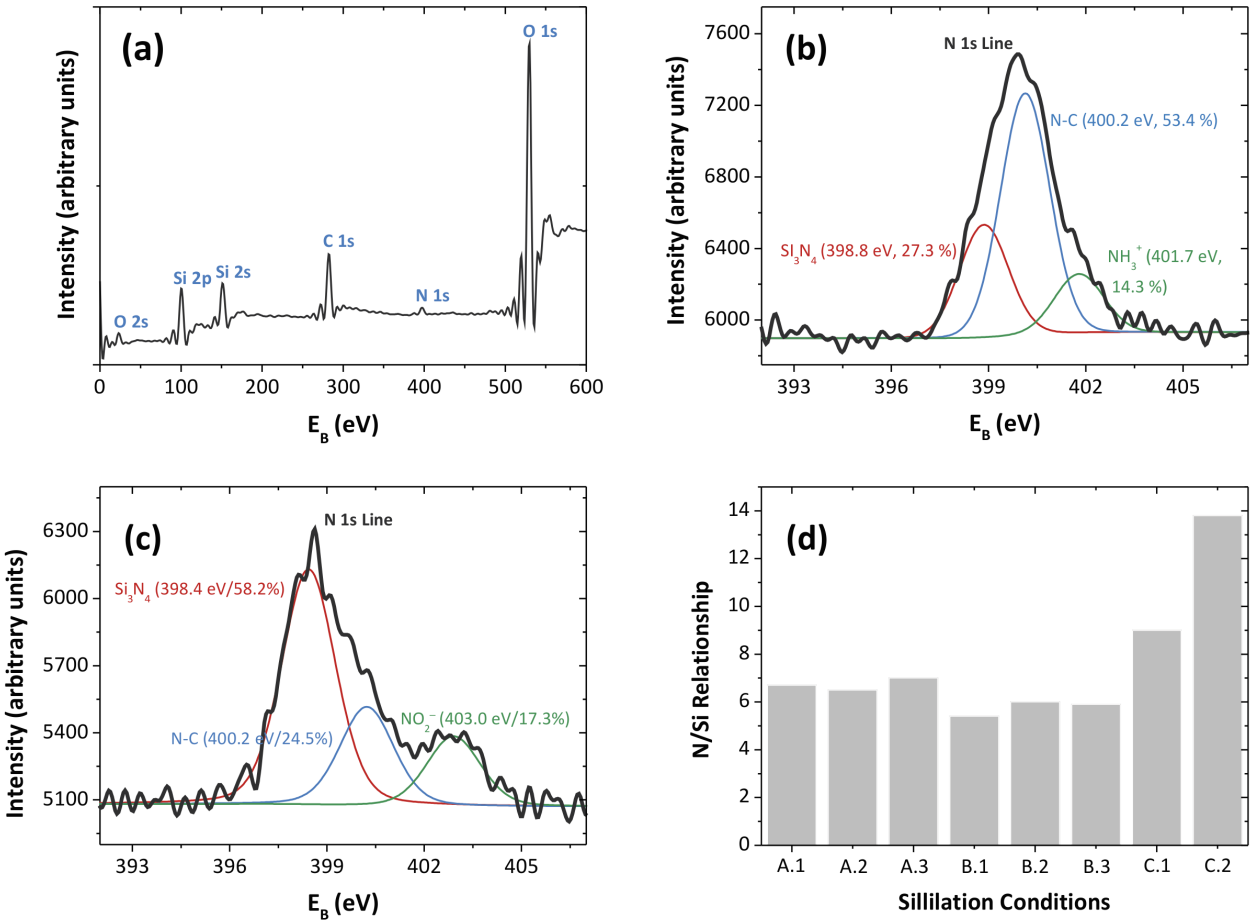

Fig. S4 Optimization of silanization conditions. XPS spectra of SiO_2 films modified with SAM C.2 (a,b) and SAM A.3 (c) and N/Si percentage relationships for all silanization conditions (d). In figures (b) and (c), the binding energies (E_B, eV) and percentage relative quantities are reported in parentheses for each component of the N 1s lines.

The substrate cleaning and drying procedures were carried out with abundant ethanol and N_2 flow, respectively. The modified SiO_2 films presented low hydration level, as shown in the Fig. S3. From this figure, we observed the absence of the Si–OH species (about 99.6 eV). In addition, the interfacial reactions for construction of the biosensor phase are shown in Fig. S5.[16,17] The $–NH_2$ group at the top of the FA molecule is its bioactive component, responding mainly by the specific interactions with FR-α whereas, in this communication, we used α-FA.

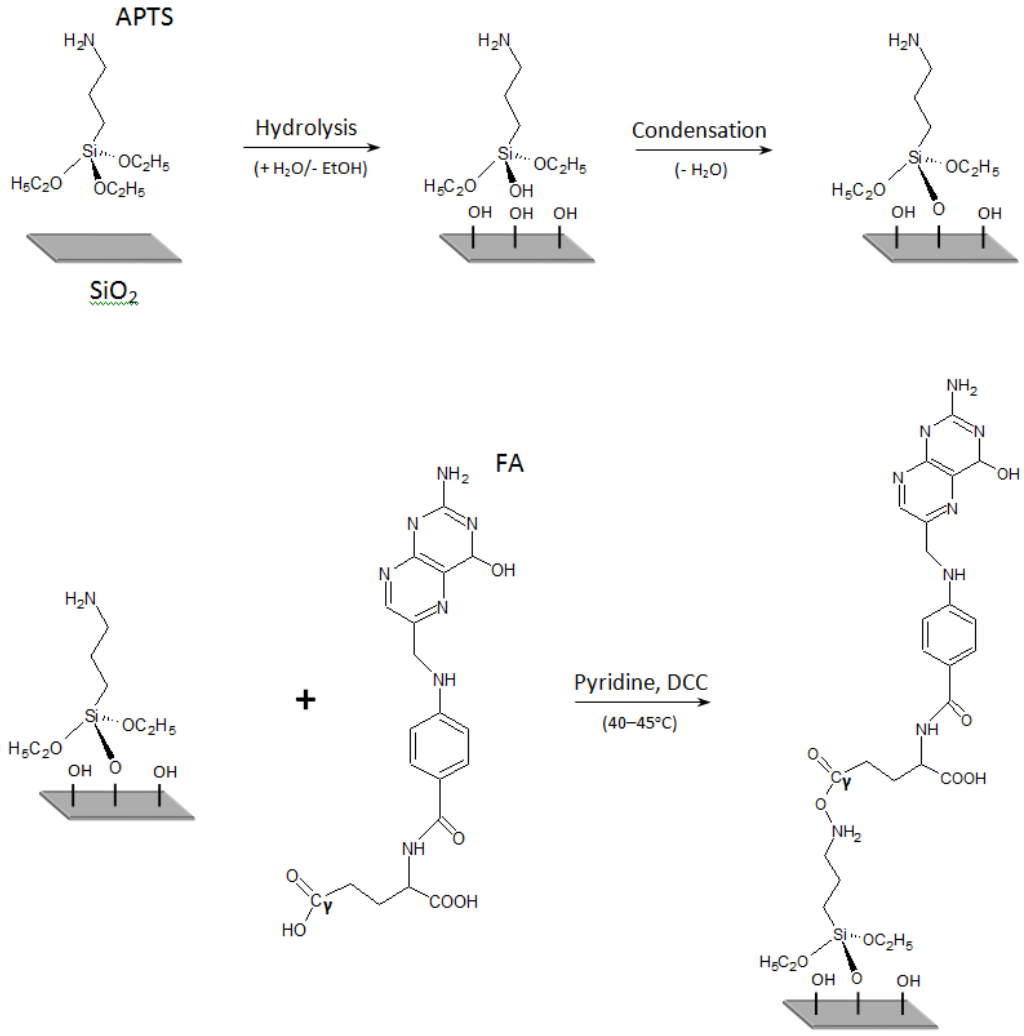

Fig. S5 Interfacial reactions for functionalization of the SiO_2 film with FA.

References

1. J. A. F. da Silva and C. L. do Lago, *Anal. Chem.*, 1998, **70**, 4339.
2. P. A. P. Nascente, *J. Mol. Catal. A: Chem.*, 2005, **228**, 145.
3. H. J. Kim, Q. Shao, Y. H. Kim, *Surface and Coatings Technology*, 2003, **171**, 39.
4. N. J. Farcich, J. Salonen, P. M. Asbeck, IEEE Transactions on Microwave Theory and Techniques, 2008, **56**, 2963.
5. R. S. Lima, T. P. Segato, A. L. Gobbi, W. K. T. Coltro, and E. Carrilho, *Lab Chip*, 2011, **11**, 4148.

6. W. K. T. Coltro, R. S. Lima, T. P. Segato, E. Carrilho, D. P. de Jesus, C. L. do Lago, and J. A. F. da Silva, *Anal. Methods*, 2012, **4**, 25.
7. P. Kubaň and P. C. Hauser, *Electrophoresis*, 2004, **25**, 3387.
8. J. Wang, M. Pumera, G. E. Collins, and A. Mulchandani, *Anal. Chem.*, 2002, **74**, 6121.
9. B. Damaskin, O. Petri, *Fundamentos da electroquímica teórica*, Moscovo: MIR, 1985.
10. A. J. Bard and L. R. Faulkner, *Electrochemical Methods: Fundamentals and Applications*, John Wiley & Sons: New York, 2001.
11. D. Halliday, R. Resnick, and J. Walker, *Fundamentals of Physics*, John Wiley & Sons: New York, 2001.
12. C. Y. Lee, C. M. Chen, G. L. Chang, C. H. Lin, and L. M. Fu, *Electrophoresis*, 2006, **27**, 5043.
13. A. Paul, *Chemistry of Glasses*. London: Chapman and Hall, 1982.
14. P, Kubáň and P. C. Hauser, *Lab on a Chip*, 2005, **25**, 407.
15. J. A. Howarter and J. P. Youngblood, *Langmuir***,** 2006**, 22**, 11142.
16. J. W. Lee, J. Y. Lu, P. S. Low, and P. L. Fuchs, *Bioorg. Medicinal Chem.*, 2002, **10**, 2397.
17. J. A. Howarter and J. P. Youngblood, *Langmuir*, 2006, **22**, 11142.